AIP Applied Physics Letters

Au impact on GaAs epitaxial growth on GaAs (111)B substrates in molecular beam epitaxy

Zhi-Ming Liao, Zhi-Gang Chen, Zhen-Yu Lu, Hong-Yi Xu, Ya-Nan Guo et al.

Citation: Appl. Phys. Lett. **102**, 063106 (2013); doi: 10.1063/1.4792053
View online: http://dx.doi.org/10.1063/1.4792053
View Table of Contents: http://apl.aip.org/resource/1/APPLAB/v102/i6
Published by the AIP Publishing LLC.

Additional information on Appl. Phys. Lett.

Journal Homepage: http://apl.aip.org/
Journal Information: http://apl.aip.org/about/about_the_journal
Top downloads: http://apl.aip.org/features/most_downloaded
Information for Authors: http://apl.aip.org/authors

ADVERTISEMENT

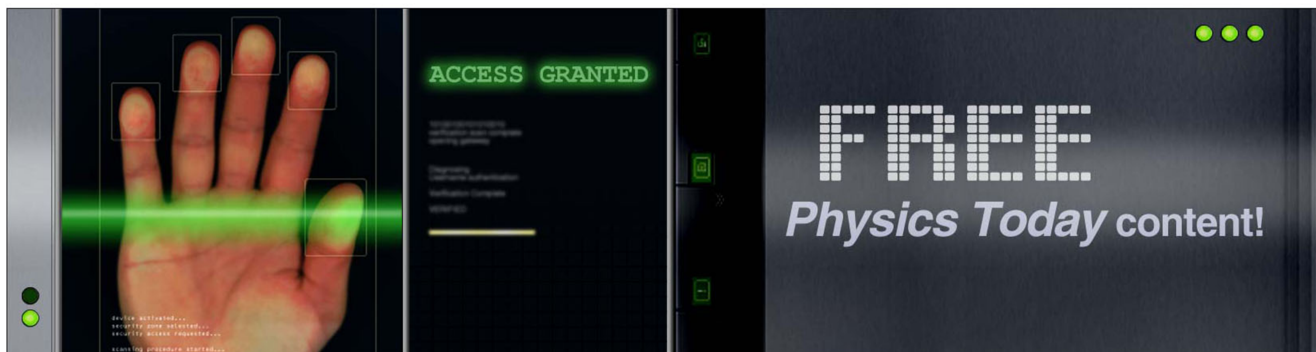

Downloaded 23 Jun 2013 to 130.102.158.24. This article is copyrighted as indicated in the abstract. Reuse of AIP content is subject to the terms at: http://apl.aip.org/about/rights_and_permissions

APPLIED PHYSICS LETTERS **102**, 063106 (2013)

Au impact on GaAs epitaxial growth on GaAs $(111)_B$ substrates in molecular beam epitaxy

Zhi-Ming Liao,[1] Zhi-Gang Chen,[1] Zhen-Yu Lu,[2] Hong-Yi Xu,[1] Ya-Nan Guo,[1] Wen Sun,[1] Zhi Zhang,[1] Lei Yang,[1] Ping-Ping Chen,[2] Wei Lu,[2] and Jin Zou[1,3,a)]

[1]*Materials Engineering, The University of Queensland, St. Lucia, Queensland 4072, Australia*
[2]*National Laboratory for Infrared Physics, Shanghai Institute of Technical Physics, Chinese Academy of Sciences, 500 Yu-Tian Road, Shanghai 200083, People's Republic of China*
[3]*Centre for Microscopy and Microanalysis, The University of Queensland, St. Lucia, Queensland 4072, Australia*

(Received 14 November 2012; accepted 30 January 2013; published online 12 February 2013)

GaAs growth behaviour under the presence of Au nanoparticles on GaAs $\{111\}_B$ substrate is investigated using electron microscopy. It has been found that, during annealing, enhanced Ga surface diffusion towards Au nanoparticles leads to the GaAs epitaxial growth into $\{113\}_B$ faceted triangular pyramids under Au nanoparticles, governed by the thermodynamic growth, while during conventional GaAs growth, growth kinetics dominates, resulting in the flatted triangular pyramids at high temperature and the epitaxial nanowires growth at relatively low temperature. This study provides an insight of Au nanoparticle impact on GaAs growth, which is critical for understanding the formation mechanisms of semiconductor nanowires. © *2013 American Institute of Physics.* [http://dx.doi.org/10.1063/1.4792053]

Rational design and fabrication of semiconductor nanowires as building blocks for functional materials and devices are the key to tailoring properties for specific applications in future electronic and optoelectronic devices,[1–3] such as chemical and biological sensors,[4] electronics,[5,6] and lasers.[7] Fundamental understanding of the catalyst behaviours in the fabrication of nanowires will further enable the rational growth of nanowires. It has been well documented that vapor-liquid-solid (VLS) mechanism[8] is an effective approach to grow nanowires. Especially, metallic nanoparticles used to assist nanowire growth as catalysts in the VLS model, together with their physical and chemical characteristics, play a key role in determining the crystal structures, chemical compositions, and orientations of nanowires.[9,10] Different metal nanoparticles, such as Au,[11] Fe,[12] Pt,[13] Pd,[14] and Ga[15] have been used to catalyst nanowire growth.[16] Among all kinds of metallic catalysts, Au has been commonly used to catalyze the growth of semiconductor nanowires[9,17] and nanowire heterostructures.[18–20] There are several approaches to prepare Au catalysts, such as aerosol-generated Au particles,[21] colloidal Au particles,[22,23] electron beam lithography defined Au particles,[24] and Au particles generated by annealing of thin films.[25,26] Of these approaches, the thin film generated Au nanoparticles (TFA) is a simple and cost-effective approach, in which the Au nanoparticles are realized by decomposition of the Au thin films into nanoparticles during annealing process. Simultaneously, the annealing may remove the surface oxidation in order to obtain a pristine surface and may form alloyed droplets for catalyzing semiconductor nanowires. For nanowires catalyzed by the TFA particles to be practically useful, it is necessary to fundamentally understand the Au behaviour on the semiconductor substrates before nanowire growth, which is critical for understanding the formation mechanisms of semiconductor nanowires. In the case of annealing Au thin films on Si (001) substrates, complex Au-Si droplet behaviour and different surface nanostructures have been observed.[27,28] On the other hand, the structural behaviour of interfaces between Au thin films and GaAs substrates has been investigated because this system has been consequently used as ohmic contacts.[29,30] However, detailed role of Au nanoparticles on the GaAs surfaces during the annealing is not clear, although the evolution of Au containing droplets in Au coated GaAs substrates depends strongly upon the environmental conditions. As a consequence, it is critical to determine the Au behaviour from view-points of fundamental understanding and technological applications.

In this study, we investigated the Au behaviour during the annealing of Au coated GaAs $(111)_B$ substrate, and consequent growth of GaAs at different temperatures in a molecular beam epitaxy (MBE) system. Since the formation of Au alloyed nanoparticles can be a complex process, the employment of the high-vacuum MBE system will minimize the potential contamination and thus simplify the complexity. By carefully designed experiments, we demonstrate extraordinary surface nanostructures formed during annealing and evolved by consequent GaAs growth. Through detailed structural characterization by using electron microscopy, the formation mechanism of the observed surface nanostructure is explored.

Three samples of Au thin film coated GaAs $\{111\}_B$ substrates were prepared in a Riber 32 MBE system. For sample A, a 500 nm thick GaAs buffer layer was first grown on the GaAs $\{111\}_B$ substrate at 550 °C to improve the surface smoothness. After that, the substrate was transferred into the deposition chamber, and a ~0.5 nm thick Au thin film was then deposited on the top of the GaAs buffer layer by the vacuum thermal evaporation. The Au coated GaAs was then transferred to the MBE's growth chamber and the annealing was carried out at 550 °C in the As ambient for 5 min. After

a)Email: j.zou@uq.edu.au.

 © 2013 American Institute of Physics

Downloaded 23 Jun 2013 to 130.102.158.24. This article is copyrighted as indicated in the abstract. Reuse of AIP content is subject to the terms at: http://apl.aip.org/about/rights_and_permissions

the annealing, the sample was cooled down to room temperature naturally under the As ambient. For samples B and C, identical procedure was carried out except, after annealing, the growth of GaAs was carried out at 500 °C for 60 min for sample B and at 350 °C for 20 s for sample C, respectively, both with a V/III ratio of 40.

The morphological characteristics of annealed and grown nanostructures were investigated by scanning electron microscopy (SEM, JEOL 7001 F, operated at 15 kV), and their detailed structural and chemical characteristics were characterized using transmission electron microscopy [TEM, Philips Tecnai F20, operated at 200 kV, equipped with energy dispersive spectroscopy (EDS)]. The cross-section TEM specimens were prepared by first mechanical thinning, followed by ion-beam thinning using a Gatan precision ion polishing system.

Figure 1 shows typical SEM images of three samples, viewed from the top (the electron beam is parallel to the surface normal) and from the side (the electron beam is almost parallel to the surface with a slightly tilt in order to determine the lateral distribution of the Au nanoparticles). Figure 1(a) is a top-view SEM image of sample A, in which randomly distributed Au nanoparticles with a size of ∼30 nm can be observed. It is of interest to note that a triangular base with a size of ∼100 nm can be found under each Au nanoparticle. Figure 1(b) is a side-view SEM image of sample A, and shows trapezium base under the Au nanoparticles. Taking both the top-view and side-view SEM observations into account, it is anticipated that the base under each Au nanoparticle has a triangular pyramid shape. Figures 1(c) and 1(d) are typical SEM images taken from sample B, viewed, respectively, from top and side, and show similar morphological characteristics. The comparison of SEM images taken from two samples indicates that the additional GaAs growth at high temperature mainly led to the growth of pyramid bases, especially laterally, as the lateral dimension of pyramid bases in sample B has approached to 1 μm. Figures 1(e) and 1(f) are top-view and side-view SEM images taken from sample C. The comparison between Figs. 1(a) and 1(e) indicates that the pyramid bases in sample C have similar morphology as those in sample A. However, the side-view SEM image shows short nanowires, meaning that the relatively low growth temperature leads to the one-dimensional nanowire growth.

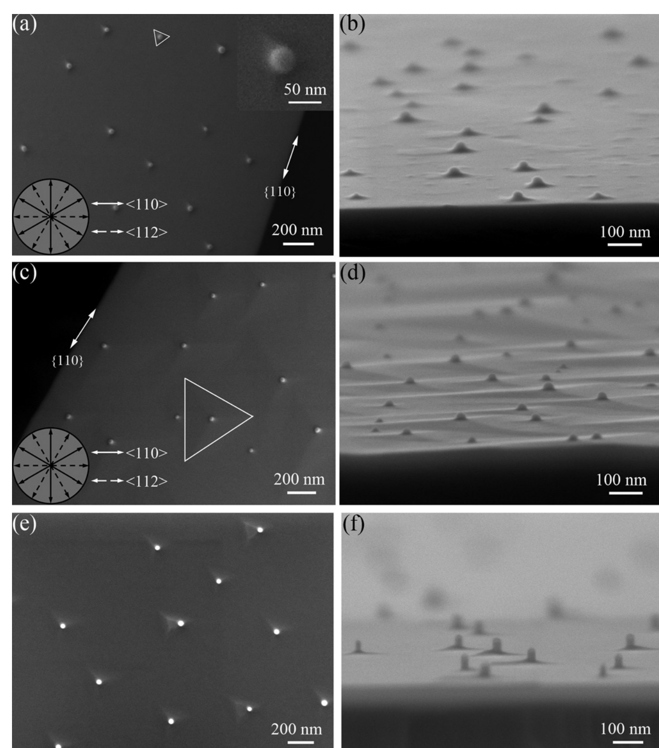

FIG. 1. SEM images taken from samples A, B, and C, viewed from the top [(a), (c), and (e)] and from the side [(b), (d), and (f)].

It is well documented that the natural cleavage plane of zinc-blende GaAs is {110} planes,[31] which can be used to determine the crystal orientation of triangular pyramids. By comparing the triangles with the {110} cleavages shown in Figs. 1(a) and 1(c), their crystallographic orientation relationship can be determined. In these two top-view SEM images, the bottom edges of triangular pyramids are paralleled to ⟨110⟩ directions on the substrate surface. Based on this information, the facets of truncated triangular pyramids in both samples can be determined as {11 N} planes with N being an integer.

To determine the detailed structural and chemical characteristics of obtained nanostructures, cross-sectional TEM investigations were performed. Figure 2(a) is a low-magnification cross-sectional TEM image of sample A, and shows that the surface between pyramid-like bases is flat, indicating that there are no island/layer overgrowths on the substrate except pyramid bases underneath the Au nanoparticles. Figure 2(b) is a ⟨110⟩ high-resolution TEM image of a typical Au nanoparticle with a pyramid base underneath, in which a hemisphere-shaped Au nanoparticle is seen, under which two sections can be realized between the Au nanoparticle and the substrate surface. Incorporated with SEM investigation, section I can be deduced as a triangular pyramid with ∼20 nm in height, and section II is ∼15 nm in height with relatively vertical sides. Figure 2(c) is a low-magnification cross-sectional TEM image of sample B, showing gentle undulating surface. The comparison between Figs. 1(d) and 2(c) suggests the observed undulating surface is caused by relatively flat triangular pyramids under Au nanoparticles, which correspond to section I in sample A. Figure 2(d) is a ⟨110⟩ high-resolution TEM image of a typical Au nanoparticle with induced nanostructure underneath, where a GaAs section of ∼15 nm in height is seen, which has a similar morphology with section II in Fig. 2(b). The insets in Figs. 2(b) and 2(d) are selected area electron diffraction patterns taken along the ⟨110⟩ zone axis from both samples, confirming that the crystal structure of both sections is zinc-blende structure (same as the crystal structure of the substrates), and has the identical crystallographic orientation with the substrate, so that the growth of sections I and II is truly epitaxial. Figure 2(e) is a ⟨110⟩ high-resolution TEM image of a typical nanowire in sample C and Fig. 1(f) is the corresponding fast Fourier transform (FFT), in which a ∼30 nm wurtzite structured nanowire section is epitaxially grown on a zinc-blend structured pyramid base [incorporated in Fig. 1(e)]. By comparing with samples A and B, the distinct feature of sample C is that no section II is found in the nanowires.

To determine N, we note the asymmetrical projected angles of section I with its underlying GaAs substrate shown

Downloaded 23 Jun 2013 to 130.102.158.24. This article is copyrighted as indicated in the abstract. Reuse of AIP content is subject to the terms at: http://apl.aip.org/about/rights_and_permissions

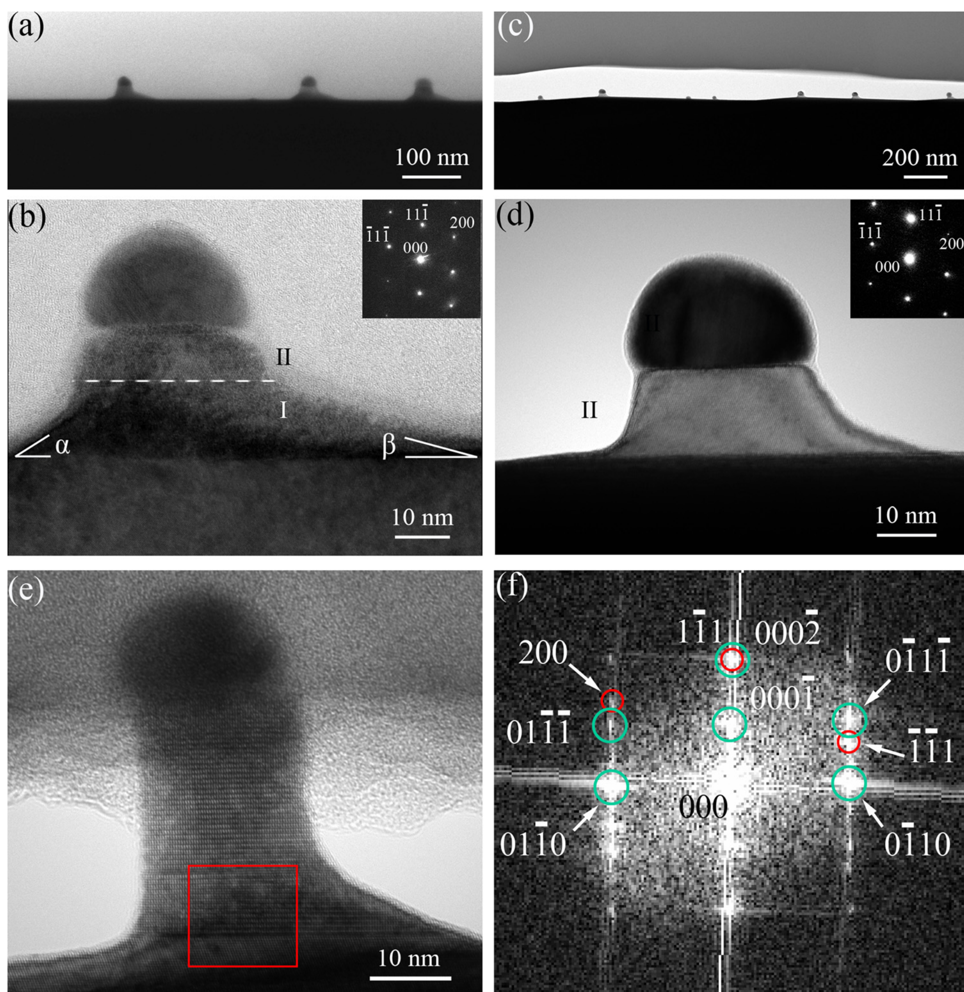

FIG. 2. (a) Cross-sectional TEM image taken from sample A; (b) $\langle 110\rangle$ cross-sectional high-resolution TEM image taken from a typical Au nanoparticle from sample A; (c) and (d) Cross-sectional TEM image and $\langle 110\rangle$ cross-sectional high-resolution TEM image of a typical Au nanoparticle, both taken from sample B. Insets in (b) and (d) showing electron diffraction patterns of zinc-blende structure; (e) $\langle 110\rangle$ cross-sectional high-resolution TEM image taken from sample C and (f) being a FFT taken at the nanowire/base interface.

in Fig. 2(b) [note that Fig. 2(b) is taken along a $\langle 110\rangle$ zone axis from a cross-section TEM specimen]. From Fig. 2(b), $\alpha \approx 30°$ and $\beta \approx 16°$ can be measured. By crystallographic calculation, facets of the triangular pyramid surfaces in sample A can be determined as $\{\bar{1}\bar{1}\bar{3}\}$, with the edge of any two adjunct $\{\bar{1}\bar{1}\bar{3}\}$ planes being along $\langle\bar{1}\bar{1}\bar{4}\rangle$. Based on this analysis, a three-dimensional structural model for the triangular pyramids from sample A can be drawn, and illustrated in Fig. 3(a). In this model, two sections observed in sample A are shown: at the bottom, a $\{\bar{1}\bar{1}\bar{3}\}$ faceted triangular pyramid standing on the substrate. Above that, section II is shown under the Au nanoparticle. Figure 3(b) shows the projection of the model along a $\langle 110\rangle$ direction, in which the projected angles are in excellent agreement with measured α and β. For sample B, the projected angles in cross-sectional TEM images are small and vary, as shown in Fig. 2(c), which cannot be assigned with any specific crystal facets, indicating that, after the additional GaAs growth at high temperature, although triangular pyramids remain, but the facets disappear.

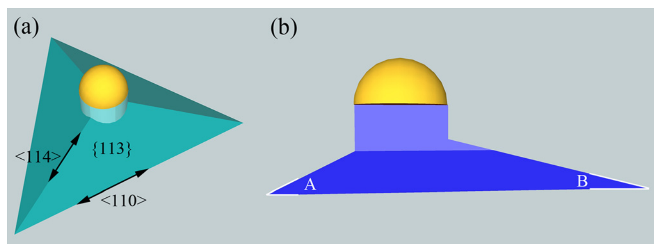

FIG. 3. (a) Schematic illustration of a three-dimensional model of the observed faceted triangular pyramid base; (b) $\langle 110\rangle$ projected model.

To understand the formation of triangular pyramids [section I shown in Fig. 2(b)], two issues need to be addressed. The first issue is how and why a large amount of Ga is attracted to the Au nanoparticles under the As ambient at 500 °C. The second issue is why $\{\bar{1}\bar{1}\bar{3}\}$ surface facets are formed as triangular pyramid bases in sample A. To address the first issue, we note that, due to the easy evaporation of As from the GaAs substrate, particular at high temperature (>500 °C), the bounding of Ga atoms to the GaAs substrate becomes loose, leading to easy surface diffusion of Ga atoms.[32] In our case, the annealing temperature was 550 °C, so that strong Ga atoms surface diffusion is expected. Meanwhile, it has been reported that (1) Au may attract a large amount of Ga even at 250 °C,[33] and (2) the maximum diffusion length of Ga atoms on GaAs $\{111\}_B$ surface has been estimated at ~5 μm at 500 °C,[34] so that a significant amount of Ga atoms can be attracted towards to the Au nanoparticles at the annealing temperature of 550 °C. It should be noted that, in our study, the Au was deposited on the GaAs buffer layer within the MBE system, the surface of GaAs buffer layer must be clear from possible oxidation, which makes the surface diffusion of Ga atoms much easier. To address the

Downloaded 23 Jun 2013 to 130.102.158.24. This article is copyrighted as indicated in the abstract. Reuse of AIP content is subject to the terms at: http://apl.aip.org/about/rights_and_permissions

second issue, we anticipate that, at the initial stage, Au nanoparticles absorb Ga to form Au-Ga alloys. When the Ga concentration in the alloy reaches to a certain level, the Au-Ga alloys become droplets. After the saturation is met with increasing Ga in the droplets, no further Ga can be absorbed by the droplets. In the presence of As vapour, the remaining aggregated Ga forms GaAs crystals with As vapour on the GaAs substrate epitaxially. According to crystallography of the zinc-blende structure, $\{113\}_B$ facets have relatively low surface energy under As-rich environment.[35] In the case of growing aggregated GaAs on $\{111\}_B$ surface epitaxially, formation of $\{113\}_B$ surface facets is then thermodynamically preferred, in which the Ga source comes only from the Ga surface diffusion. For the $\{111\}_B$ surface, 3 possible equivalent $\{113\}_B$ surface facets formed as triangular pyramids. Specifically, the $(\bar{1}\bar{1}\bar{3})$, $(\bar{1}\bar{3}\bar{1})$, and $(\bar{3}\bar{1}\bar{1})$ surface facets should be formed on the $(\bar{1}\bar{1}\bar{1})$ surface. When Ga source is switched on after the annealing (in the case of sample B), GaAs growth takes place, preferentially on the entire $(\bar{1}\bar{1}\bar{1})$ surface. It is necessary to note that, at high growth temperatures, the GaAs growth dominates through the two-dimensional growth over the one-dimensional nanowire growth.[36] Due to the pre-existing $\{113\}_B$ faceted triangular pyramids associated with Au droplets, GaAs growth tends to flat the pyramids since we believe that, in this case, the GaAs growth is governed by kinetics (under high temperature growth and strong Ga supply), resulting in flatted but extended triangular pyramids, as shown in Figs. 1(d) and 2(c). On the other hand, the similarity of pyramid bases found in samples A and C suggests that the comparatively low temperature growth can substantially restrict Ga surface diffusion.

Another remarkable fact is that the morphological and structural characteristics of section II for samples A and B are almost identical. This suggests that the formation of this section should take place under similar condition. Taking this and the fact that the section II is formed last into account, we anticipate that section II is formed during the cooling after annealing or the growth process.[37] During the natural cooling under the As ambient, the Ga in the Au-Ga alloyed droplets is expelled from the droplets and reacts with As to form GaAs on top of their underlying substrate (in this case, the top of the triangular pyramids). It is of interest to note that no section II is found in sample C. To understand this, we carried out extensive EDS analyses for the catalysts. It has been determined that the Ga concentrations in the post growth catalysts are ∼10 at. % and ∼50 at. % for samples A and C, respectively. Since the catalysts in both cases experience the same annealing process (so that the same amount of Ga in the catalysts is expected after annealing), the disappearance of section II in sample C indicates that the Ga expelled from the Au-Ga alloyed droplets only takes place when the growth finishes at relatively high temperature, and the Ga expel should terminate by ∼ 350 °C.

Based on the above analysis, the formation mechanisms of how Au nanoparticles catalyzed epitaxial GaAs growth on the $\{111\}_B$ substrate can be proposed as follows, as schematically illustrated in Fig. 4. When a thin layer of Au deposited on the GaAs $\{111\}_B$ substrate (as shown in stage I in Figure 4) is annealed, the Au film spontaneously breaks up into small particles. Simultaneously, Ga atoms on the surface diffuse into these Au nanoparticles to form Au-Ga alloys. When Ga concentration in the Au-Ga alloy is sufficient, the Au-Ga alloy nanoparticles transform into droplets, and eventfully, Ga concentration in the droplets saturates (as shown in stage II in Fig. 4). At same time, the aggregated Ga reacts with As, and forms GaAs near the Au droplets. Under

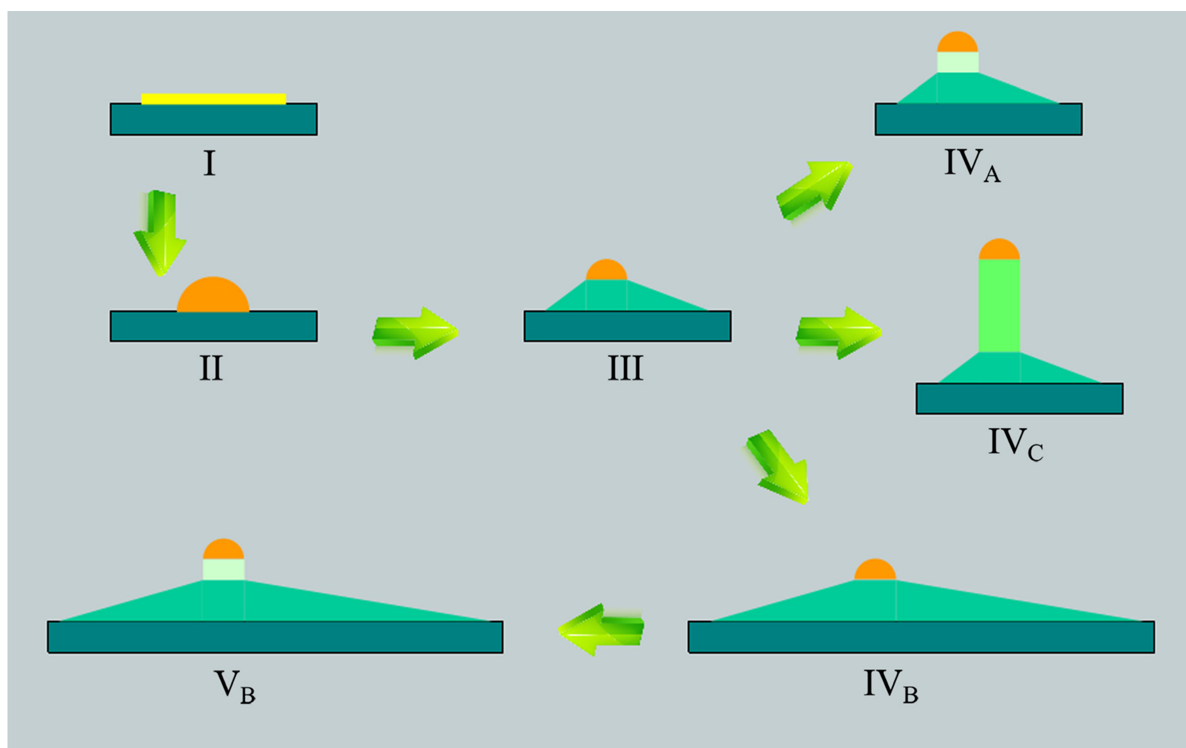

FIG. 4. Schematic diagram of how a spontaneously formed Au nanoparticle affects the formation of epitaxially grown GaAs during annealing (Ga source absent) and GaAs growth (with Ga source).

Downloaded 23 Jun 2013 to 130.102.158.24. This article is copyrighted as indicated in the abstract. Reuse of AIP content is subject to the terms at: http://apl.aip.org/about/rights_and_permissions

the limited Ga source, the GaAs growth is governed by the thermodynamics and crystallographic requirement, leading to the formation of $\{113\}_B$ faceted triangular pyramids (as shown in stage III in Fig. 4). When natural cooling is applied (in the case of sample A), Ga in the Au-Ga droplets is expelled, and reacts with As to form a small section of GaAs under the droplets (as shown in stage IV_A in Fig. 4). If the GaAs growth takes place after the annealing, flatted triangular pyramids under Au droplets are obtained (as shown in stage IV_B in Fig. 4) under relatively high growth temperature (in the case of sample B), while epitaxial nanowires will be grown (as shown in stage IV_C in Fig. 4) under relatively low growth temperature (in the case of sample C). The consequent cooling of high-temperature growth will lead to the formation of GaAs under the droplets (as shown in stages V_B in Fig. 4).

In conclusion, through carefully designed experiment (the potential surface oxidation was minimized by carrying our Au film deposition and annealing/growth in vacuum), the intrinsic impact of the existence of Au nanoparticles on GaAs $\{111\}_B$ substrate in GaAs growth is uncovered. It is found that, during annealing, Ga surface diffusion towards Au nanoparticles leads to the formation of $\{113\}_B$ faceted triangular pyramids under Au nanoparticles—thermodynamically dominated growth. For low temperature subsequent GaAs growth, the epitaxial GaAs nanowires are induced on these faceted pyramids bases, while for the subsequent high temperature GaAs growth, two-dimensional growth dominated and the faceted triangular pyramids are flatted. The final cooling after high-temperature process leads to Ga in the Au-Ga alloy droplets expelled and forms a short section of GaAs under the droplets. This finding provides a new insight of how the existence of Au nanoparticles affects the GaAs growth, which is essential for ultimately understanding the nanowire growth.

This study was financially supported by the Australian Research Council, the National Basic Research Program of China (Grant No. 2011CB925604), and the National Science Foundation of China (Grant Nos. 91021015 and 10990103). Australian Microscopy & Microanalysis Research Facility is also gratefully acknowledged for providing microscopy facilities for this study.

[1]A. I. Hochbaum and P. D. Yang, Chem. Rev. **110**, 527 (2010).
[2]Z. G. Chen, L. N. Cheng, H. Y. Xu, J. Z. Liu, J. Zou, T. Sekiguchi, G. Q. Lu, and H. M. Cheng, Adv. Mater. **22**, 2376 (2010).
[3]J. H. Kang, Q. Gao, H. J. Joyce, H. H. Tan, C. Jagadish, Y. Kim, D. Y. Choi, Y. Guo, H. Xu, J. Zou, M. A. Fickenscher, L. M. Smith, H. E. Jackson, and J. M. Yarrison-Rice, Nanotechnology **21**, 035604 (2010).
[4]Y. Cui, Q. Q. Wei, H. K. Park, and C. M. Lieber, Science **293**, 1289 (2001).
[5]H. Bi and R. R. LaPierre, Nanotechnology **20**, 465205 (2009).
[6]C. P. T. Svensson, T. Martensson, J. Tragardh, C. Larsson, M. Rask, D. Hessman, L. Samuelson, and J. Ohlsson, Nanotechnology **19**, 305201 (2008).
[7]X. F. Duan, Y. Huang, R. Agarwal, and C. M. Lieber, Nature **421**, 241 (2003).
[8]R. S. Wagner and W. C. Ellis, Appl. Phys. Lett. **4**, 89 (1964).
[9]H. J. Joyce, Q. Gao, H. H. Tan, C. Jagadish, Y. Kim, X. Zhang, Y. N. Guo, and J. Zou, Nano Lett. **7**, 921 (2007).
[10]C. Y. Wen, M. C. Reuter, J. Bruley, J. Tersoff, S. Kodambaka, E. A. Stach, and F. M. Ross, Science **326**, 1247 (2009).
[11]K. Hiruma, K. Haraguchi, M. Yazawa, Y. Madokoro, and T. Katsuyama, Nanotechnology **17**, S369 (2006).
[12]J. L. Johnson, Y. H. Choi, and A. Ural, J. Vac. Sci. Technol. B **26**, 1841 (2008).
[13]Y. S. Zhou, K. Wang, W. H. Han, S. C. Rai, Y. Zhang, Y. Ding, C. F. Pan, F. Zhang, W. L. Zhou, and Z. L. Wang, ACS Nano **6**, 6478 (2012).
[14]H. Y. Xu, Y. Wang, Y. N. Guo, Z. M. Liao, Q. Gao, H. H. Tan, C. Jagadish, and J. Zou, Nano Lett. **12**, 5744 (2012).
[15]B. Bauer, A. Rudolph, M. Soda, A. F. I. Morral, J. Zweck, D. Schuh, and E. Reiger, Nanotechnology **21**, 435601 (2010).
[16]N. Jungwirth, E. Dailey, P. Madras, and J. Drucker, J. Vac. Sci. Technol. B **29**, 061805 (2011).
[17]M. E. Messing, K. Hillerich, J. Johansson, K. Deppert, and K. A. Dick, Gold Bull. **42**, 172 (2009).
[18]M. Paladugu, J. Zou, Y. N. Guo, G. J. Auchterlonie, H. J. Joyce, Q. Gao, H. H. Tan, C. Jagadish, and Y. Kim, Small **3**, 1873 (2007).
[19]Y. N. Guo, J. Zou, M. Paladugu, H. Wang, Q. Gao, H. H. Tan, and C. Jagadish, Appl. Phys. Lett. **89**, 231917 (2006).
[20]M. Paladugu, J. Zou, Y. N. Guo, X. Zhang, Y. Kim, H. J. Joyce, Q. Gao, H. H. Tan, and C. Jagadish, Appl. Phys. Lett. **93**, 101911 (2008).
[21]P. Caroff, M. E. Messing, B. M. Borg, K. A. Dick, K. Deppert, and L. E. Wernersson, Nanotechnology **20**, 495606 (2009).
[22]A. I. Hochbaum, R. Fan, R. R. He, and P. D. Yang, Nano Lett. **5**, 457 (2005).
[23]Y. Kim, H. J. Joyce, O. Gao, H. H. Tan, C. Jagadish, M. Paladugu, J. Zou, and A. A. Suvorova, Nano Lett. **6**, 599 (2006).
[24]T. Martensson, M. Borgstrom, W. Seifert, B. J. Ohlsson, and L. Samuelson, Nanotechnology **14**, 1255 (2003).
[25]H. Y. Xu, Y. Wang, Y. N. Guo, Z. M. Liao, Q. Gao, N. Jiang, H. H. Tan, C. Jagadish, and J. Zou, Cryst. Growth Des. **12**, 2018 (2012).
[26]J. C. Harmand, G. Patriarche, N. Pere-Laperne, M. N. Merat-Combes, L. Travers, and F. Glas, Appl. Phys. Lett. **87**(20), 203101 (2005).
[27]Y. M. Shao, T. X. Nie, Z. M. Jiang, and J. Zou, Appl. Phys. Lett. **101**, 053104 (2012).
[28]F. Ruffino, L. Romano, G. Pitruzzello, and M. G. Grimaldi, Appl. Phys. Lett. **100**, 053102 (2012).
[29]N. Braslau, J. B. Gunn, and J. L. Staples, Solid-State Electron. **10**, 381 (1967).
[30]J. S. Harris, Y. Nannichi, and G. L. Pearson, J. Appl. Phys. **40**, 4575 (1969).
[31]A. R. Lubinsky, C. B. Duke, B. W. Lee, and P. Mark, Phys. Rev. Lett. **36**, 1058 (1976).
[32]J. R. Arthur, J. Appl. Phys. **39**, 4032 (1968).
[33]A. K. Sinha and J. M. Poate, Appl. Phys. Lett. **23**, 666 (1973).
[34]Y. Nomura, Y. Morishita, S. Goto, Y. Katayama, and T. Isu, Appl. Phys. Lett. **64**, 1123 (1994).
[35]J. Platen, A. Kley, C. Setzer, K. Jacobi, P. Ruggerone, and M. Scheffler, J. Appl. Phys. **85**, 3597 (1999).
[36]J. Johansson, C. P. T. Svensson, T. Martensson, L. Samuelson, and W. Seifert, J. Phys. Chem. B **109**, 13567 (2005).
[37]A. I. Persson, M. W. Larsson, S. Stenstrom, B. J. Ohlsson, L. Samuelson, and L. R. Wallenberg, Nat. Mater. **3**, 677 (2004).

Downloaded 23 Jun 2013 to 130.102.158.24. This article is copyrighted as indicated in the abstract. Reuse of AIP content is subject to the terms at: http://apl.aip.org/about/rights_and_permissions